No-Load Voltage Waveform Optimization and Damper Bars Heat Reduction of Tubular Hydrogenerator by Different Degree of Adjusting Damper Bar Pitch and Skewing Stator Slot

Zhen-nan Fan, Yong Liao, Li Han, and Li-dan Xie

***Abstract*—To analyze the influence of no-load voltage waveforms and damper bar losses and heat by the damper bar pitch and stator slot skew, finite-element model (FEM) computations are conducted. The calculation models are multislice moving electromagnetic field-circuit coupling model for the hydrogenerator and three-dimensional temperature field FEM for the rotor. This analysis considers the factors such as the rotor motion and the nonlinearity of time-varying electromagnetic field, the anisotropic heat conduction of the rotor core lamination, and the different heat dissipation conditions on the windward and the leeward sides of the poles. Then, the no-load voltage waveforms of a 36 MW tubular hydrogenerator are optimized and the damper bar heat at the rated load is reduced with the design scheme by adjusting the damper bar pitch and the stator slot skew. The results show that the waveforms of the no-load voltage are improved and the temperature of damper bars are reduced when reasonably increasing damper bar pitch and skewing stator slots. The calculated results are well coincident with the test data. The research is helpful for improving the design standard and enhancing the operation reliability of the large tubular hydrogenerator and electric network.**

***Index Terms*—Damper bar heat, electromagnetic and temperature field, finite element analysis, hydrogenerator, voltage harmonic analysis.**

I. Introduction

As an important source of power energy, the voltage quality of hydrogenerator has important influence on the safe operation of power grid and electrical equipment, especially the distortion of no-load voltage waveforms, which not only aggravate the losses and heat of equipments, but also may cause false action of relay protection equipment. As an important part of hydrogenerator, damper windings are the important protection of safe and stable operation of generator and grid. The geometric structure of damper windings influences the no-load voltage waveforms and the distribution of losses and heat in the dampers. The tubular hydrogenerator is a good type of generator which is suitable for exploiting and utilizing the hydraulic resources with low water head and large flow rate [1]. However, its air gap is small, its speed is slow, and its number of slots per pole per phase is small. In the period of design, manufacturing and operation, the engineers will usually face the problems such as the bad quality of no-load voltage waveforms influenced by the tooth harmonic electro motive force (EMF), and the damper bar overheat at the rated condition [2]. In order to optimize the power quality of electricity, and ensure the safe operation of generator and grid, it is necessary to do the in-depth study of combining the optimizing of no-load voltage of generator and losses and heat of damper bars.

In the study of optimization of no-load voltage waveform, Li [3] analyzed the improving performance of no-load voltage waveform by the method of increasing air gap, fraction slot, skewing the stator slot or rotor pole, improving the surface shape of pole shoe, moving the pole position, and changing the geometry of damper bars. These methods in the early literatures by using analytical formula had clear concept and can be understood by engineers easily. However, they are difficult to consider the factors such as the nonlinearity of the time-varying electromagnetic field, the skew of stator slot, the rotation of rotor, and the eddy current of damper bars; therefore, the accuracy of calculation needs improvement. In order to overcome the aforementioned limitations, finite element (FE) method or field-circuit coupling method is widely used in recent years. For example, the magnetic field and harmonic voltage of a 150 kW salient pole generator were calculated by the FE method [4]. The influence of the pitch of damper bar and shift of damper bar on the no-load voltage waveforms was analyzed in [5] and [6]. And considering the skew of stator slots, the voltage waveforms were analyzed based on multiloop method and FE method coupling model [7].

For analyzing the currents, losses, and heat of rotor and damper bar, Knight *et al*. [8] and [9] used a permeance model with Fourier expansion approach to predict the damper bar currents. And an analytical algorithm based on equivalent network was adopted in [10] to analyze the damper bar currents and losses when the generator is operated at the rated and the no-load conditions. In [11], a combined numerical and analytical method for the computation of unbalanced magnetic pulls,

Manuscript received February 25, 2012; revised September 1, 2012, December 18, 2012, and February 18, 2013; accepted April 3, 2013. Date of publication May 20, 2013; date of current version August 16, 2013. This work was supported by the Fundamental Research for the Central Universities under Project CDJXS11151152. Paper no. TEC-00084-2012.

Z.-n. Fan, Y. Liao, and L. Han are with the State Key Laboratory of Power Transmission Equipment and System Security and New Technology, Chongqing University, Chongqing 400030, China (e-mail: fanzhennan@126.com; liaoyong_cqu@126.com; hanli_cqu@126.com).

L.-d. Xie is with Guodian Nanjing Automation Co. Ltd., Nanjing 210003, China (e-mail: adamxie84@yahoo.com.cn).

Color versions of one or more of the figures in this paper are available online at http://ieeexplore.ieee.org.

Digital Object Identifier 10.1109/TEC.2013.2259628

TABLE I
BASIC DATA OF THE GENERATOR

Parameter	Value
Rated power (MW)	36
Rated voltage (kV)	10.5
Rated current (A)	2151
Power factor	0.92
Number of magnetic poles	72
Number of damper bars per pole	4
Number of slots per pole per phase	$1\frac{1}{2}$

TABLE II
EIGHT DESIGN SCHEMES OF STRUCTURE

Design scheme	Definition
1	t_2/t_1=0.6，no skewed slot in stator
2	t_2/t_1=0.7，no skewed slot in stator
3	t_2/t_1=0.8，no skewed slot in stator
4	t_2/t_1=0.9，no skewed slot in stator
5	t_2/t_1=0.93，0.25 slot skewed in stator
6	t_2/t_1=0.93，0.5 slot skewed in stator
7	t_2/t_1=0.93，0.75 slot skewed in stator
8	t_2/t_1=0.93，1 slot skewed in stator

damper bar currents, and losses of laminated low-speed hydrogenerators in eccentricity conditions under the no-load was proposed. In [12], the temperature field of rotor was calculated by the three-dimensional (3-D) FE model. And the rotor temperature distribution of hydrogenerator was calculated by flow field and temperature field method in [13].

In this paper, the no-load voltage waveforms of a 36 MW tubular hydrogenerator are optimized and the damper bar heat is reduced with the design scheme by adjusting the damper bar pitch and the stator slot skew, and the computations are implemented and analyzed by multislice moving electromagnetic field-circuit coupling model of the hydrogenerator and 3-D temperature field FE model of rotor.

II. CALCULATION MODELS

A. Boundary-Value Problem of Moving Electromagnetic Field

The version of the generator is SFWG36-72/7350, and the basic data of the generator are shown in Table I.

Eight different design schemes are calculated and shown in Table II, where t_1 is the stator tooth pitch, which is invariant, t_2 is the damper bar pitch. In the eight schemes, scheme 1 is the original design and scheme 6 is the practical design scheme.

According to the periodicity of magnetic field, a pair of poles is chosen as the electromagnetic field calculation region. And along the z-axis, the generator is divided into 12 slices, as shown in Fig. 1.

Considering the saturation of iron core, the governing equation of nonlinear time-varying electromagnetic moving field is [14]

$$\nabla \times (\nu \nabla \times \mathbf{A}) + \sigma \left[\frac{\partial \mathbf{A}}{\partial t} - \mathbf{V} \times (\nabla \times \mathbf{A}) \right] = \mathbf{J_S} \qquad (1)$$

where $\mathbf{A}$ is the vector magnetic potential, $\mathbf{J}_s$ is the source current density, ν is the reluctivity, $\mathbf{V}$ is the velocity, and σ is the conductivity.

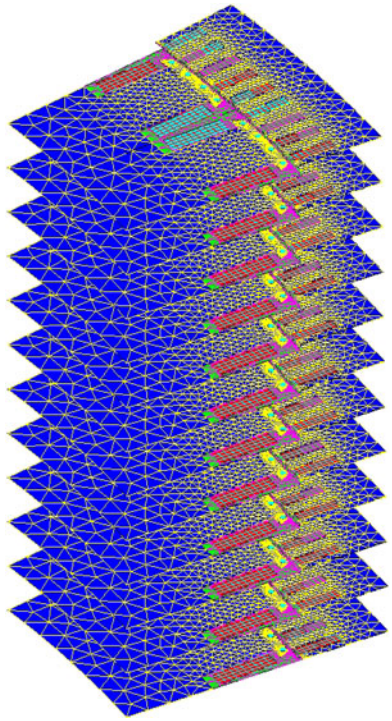

Fig. 1. Problem region and meshes of electromagnetic field.

In the multislice moving electromagnetic field model, for each slice, the current density and vector magnetic potential have only the axial z component, and the speed has only the circumferential x component. With the Coulomb norm $\nabla \cdot \mathbf{A} = 0$ and the boundary condition of the problem region, the following two-dimensional (2-D) boundary-value problem of nonlinear time-varying moving electromagnetic field for the generator is then obtained:

$$\begin{cases} \dfrac{\partial}{\partial x}\left(\nu \dfrac{\partial A_{slz}}{\partial x}\right) + \dfrac{\partial}{\partial y}\left(\nu \dfrac{\partial A_{slz}}{\partial y}\right) \\ \quad = -J_{slz} + \sigma \dfrac{\partial A_{slz}}{\partial t} + V_x \sigma \dfrac{\partial A_{slz}}{\partial x} \\ A_{slz}|_{\text{arc\_in}} = A_{slz}|_{\text{arc\_out}} = 0 \\ A_{slz}|_{\text{cyclic\_boundary\_start}} = A_{slz}|_{\text{cyclic\_boundary\_end}} \end{cases} \qquad (2)$$

where V_x is the x component of velocity, J_{slz} is the axial z component of source current density, and A_{slz} is the axial z component of vector magnetic potential.

B. Coupling Circuits

To consider the influence of the stator end winding and the rotor damper end rings, the coupling circuit models are established. The external circuit equation and electromagnetic equation should be combined in the calculation [15].

Based on the stator coupling circuit, as shown in Fig. 2, the voltage equation of stator circuit is

$$e_s = u_s + R_{1e} i_s + L_{1e} \frac{di_S}{dt} \qquad (3)$$

where e_s, u_s, and i_s are the inductive EMF, the voltage and current of the stator phase winding, respectively, R_{1e} and L_{1e} are

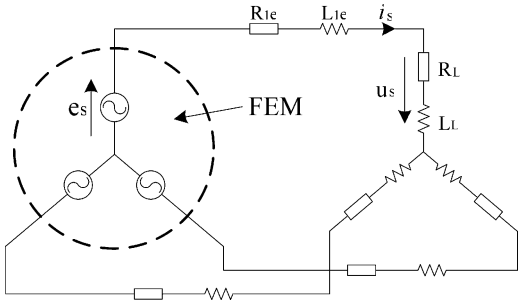

Fig. 2. Coupling circuit of the stator.

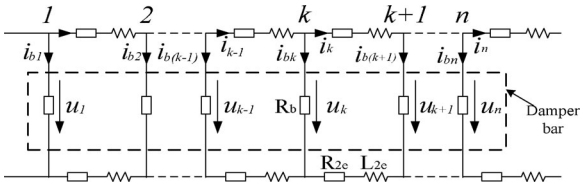

Fig. 3. Coupling circuit of the damper winding.

the resistance and leakage inductance of the stator end winding, respectively, and R_L and L_L are the resistance and inductance of loads, respectively. By changing their values, different operation conditions of generator can be set.

With the circuit of the damper winding as illustrated in Fig. 3, supposing i_{k-1} and i_k are the end ring currents of the left and right branches of kth damper bar, the relationship among i_{k-1}, i_k, and the current of damper bar i_{bk} can be obtained as follows:

$$i_k - i_{k-1} + i_{bk} = 0. \tag{4}$$

And the voltage equation to describe the relationship between kth and $(k+1)$th branches of the damper bars is given by

$$u_k - u_{k+1} = 2i_k R_{2e} + 2L_{2e}\frac{di_k}{dt} \tag{5}$$

where R_{2e} and L_{2e} are the resistance and inductance of the damper end ring, respectively.

According to the periodic condition, the constraint condition of the current and the voltage on the boundary are

$$i_1 + i_n + i_{b1} = 0 \tag{6}$$

$$u_n - u_1 = 2i_n R_{2e} + 2L_{2e}\frac{di_n}{dt} \tag{7}$$

where n is the number of damper bars in the problem region.

The stator–rotor coupling circuit equation of generator and the electromagnetic equation are combined, the magnetic vector potential A_{slz} of slices is calculated in time-step FE method, then the flux density, voltage, current, and loss can be acquired.

C. No-Load Voltage Calculation of the Generator

In Fig. 2, the no-load operating condition of the generator is simulated when the load resistance R_L and inductance L_L are infinite. By the time-step FE method, the no-load line voltage is then obtained as follows:

$$u_0 = \sqrt{3}\left(-R_{1e}i_s - L_{1e}\frac{di_s}{dt} + \frac{N_s l_{sl}}{S}\sum_{j=1}^{N_{cl}}\sum_{i=1}^{N} \times \left\{\int_{S_i^+}\int \frac{\partial A_{slzi}}{\partial t}dS - \int_{S_i^-}\int \frac{\partial A_{slzi}}{\partial t}dS\right\}\right) \tag{8}$$

where N_{cl} is the number of slices, N_s is the number of series conductors of the stator phase winding, l_{sl} is the effective length of the stator core in a layer, S is the current area of the phase winding of each slice, S_i^+ and S_i^- are the areas of a mesh where the current inflows and outflows the winding of each slice, respectively, and A_{slzi} is the average value of the vector magnetic potential in the element.

The deviation between the actual and sinusoidal waveforms of the line voltage is defined as the harmonic distortion factor (HDF), whose value is calculated according to the standard GB/T 1029-2005 [16]

$$\text{HDF} = \frac{\sqrt{U_2^2 + U_3^2 + \cdots + U_n^2}}{U_1} \times 100\%. \tag{9}$$

To weigh the disturbance for the harmonics of voltage waveform to telecommunication, the telephone harmonic factor (THF) is defined as the following according to the GB/T 1029-2005:

$$\text{THF} = \frac{\sqrt{U_1^2\lambda_1^2 + U_2^2\lambda_2^2 + \cdots + U_n^2\lambda_n^2}}{U} \times 100\% \tag{10}$$

where U is the actual line voltage, U_k ($k = 1, 2, 3, \ldots, n$, where n is the highest order considered) is the line voltage value of kth harmonic, and λ_k is the weighted coefficient of kth harmonic.

For large generators, the GB/T 1029-2005 regulated HDF $\leq 5\%$, THF $\leq 1.5\%$.

D. Loss Calculation of Damper Bars

In Fig. 2, the rated operating condition of the generator is simulated when the load resistance R_L and inductance L_L are with the rated values. In addition, owing to the assembling air gap between the damper bar and the damper slot is only about 0.15 mm, the contact resistance between the damper bars and pole core is very large. Besides, the rotor pole is laminated with silicon electrical steel sheets, and there are oxide layers on the surface of these sheets, leading to the very high resistance of pole core; therefore, the effect of currents flowing from one damper bar to the next through the pole core can be neglected.

For the jth layer of the multislice model, the eddy current density of the kth damper bar is

$$J_{jk} = -\sigma_b\frac{\partial A_{slz}}{\partial t} + \sigma_b\frac{u_k}{l_b} \tag{11}$$

where σ_b is the conductivity of damper bar, l_b is the length of damper bar, and u_k is the voltage of the kth damper bar.

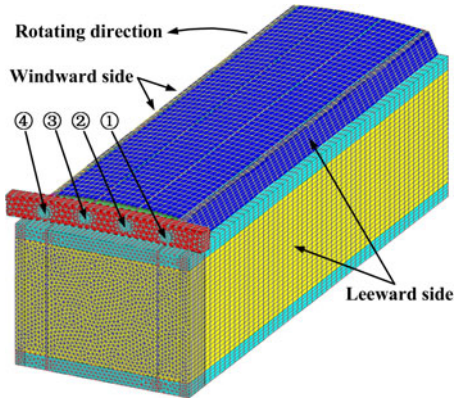

Fig. 4. Problem region of 3-D temperature field.

The current and loss of each mesh of the jth layer of damper bar are given by

$$I_e = \iint_{\Delta_e} J_{jk} dxdy \tag{12}$$

$$p_e = I_e^2 \frac{l_{bsl}}{\sigma_b \Delta_e} \tag{13}$$

where l_{bsl} is the length of the jth layer damper bar and Δ_e is the area of the related mesh of the damper bar.

The eddy current loss of one damper bar is given by

$$p_{db} = \sum_{j=1}^{N_{cl}} \sum_{e=1}^{N} p_e \tag{14}$$

where N is the number of meshes of one damper bar in each slice and N_{cl} is the slice number of model.

E. Boundary-Value Problem of Rotor 3-D Temperature Field

Because of the symmetric structure of the rotor pole and its ventilation system, the distribution of rotor temperature field is mirror symmetric on the both sides of the rotor shaft middle profile. Therefore, an half axial section of the whole rotor pole, which consists of rotor core, damper bar, field winding and its bracket, etc., is selected as the problem region for the 3D temperature field solving, and the region includes 256 256 elements, as shown in Fig. 4. There are four damper bars on each pole shoe. For easy discussion, the damper bar on the leeward side is numbered as the first and the damper bar on the windward is numbered the fourth.

Considering the anisotropic heat conduction condition of rotor core, the boundary-value problem of 3-D steady temperature field can be expressed as follows:

$$\begin{cases} \dfrac{\partial}{\partial x}\left(\lambda_x \dfrac{\partial T}{\partial x}\right) + \dfrac{\partial}{\partial y}\left(\lambda_y \dfrac{\partial T}{\partial y}\right) + \dfrac{\partial}{\partial z}\left(\lambda_z \dfrac{\partial T}{\partial z}\right) = -q_V \\ \lambda \dfrac{\partial T}{\partial n}\Big|_{S_2} = 0 \\ \lambda \dfrac{\partial T}{\partial n}\Big|_{S_3} = -\alpha(T - T_f) \end{cases} \tag{15}$$

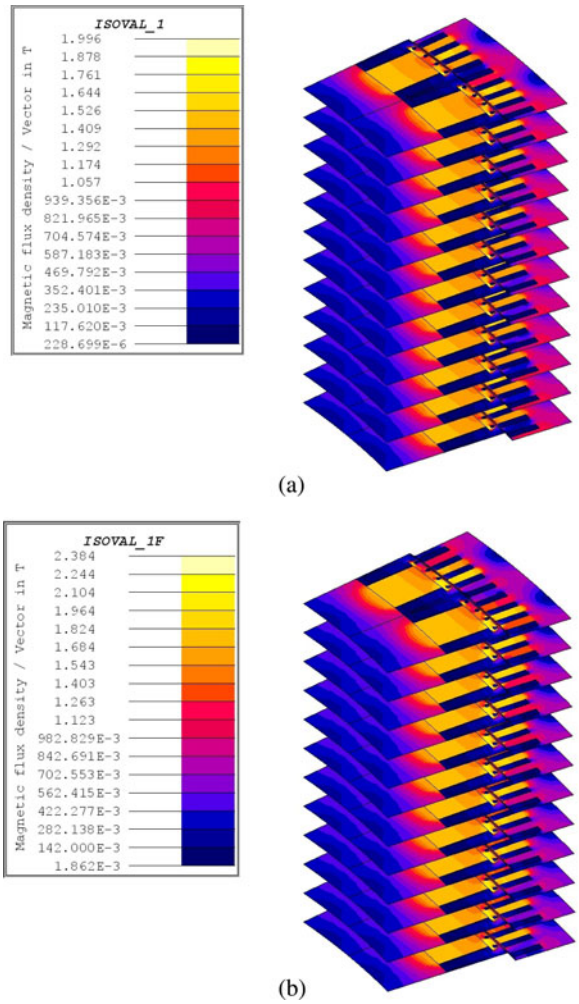

Fig. 5. Electromagnetic field distributions with no load and rated load $t_2/t_1 = 0.93$ and 0.5 slot skewed. (a) Field with no load. (b) Field with rated load.

where T is the temperature, λ_x, λ_y, and λ_z are the heat conductivity on each direction, respectively, q_v is the heat source density that is obtained by the loss calculation mentioned earlier, S_2 is the rotor middle profile and the interface between rotor core and rim related with the thermal insulation boundary condition, S_3 is the outside surface of the rotor related with the heat dissipation boundary condition, α is the heat dissipation coefficient of S_3, and T_f is the environment air temperature.

III. Computation Results and Discussions

A. Distribution of Electromagnetic Field

According to the models mentioned above the magnetic field is calculated, and the magnetic field distributions of scheme 6 are shown in Fig. 5.

Fig. 5 shows that the distributions of magnetic field of each slice are similar. When the generator operates at the no load, the distribution of the magnetic field about the center axis of the pole is symmetric. Because of the armature reaction, the distribution of the air gap magnetic field is distorted when the generator operates at the rated load. The magnetic field on the

TABLE III
HARMONICS AND QUALITY OF NO-LOAD VOLTAGE

t_2/t_1	Harmonics of no-load voltage (%)					Voltage quality	
	1	8	10	17	19	*HDF*(%)	*THF* (%)
0.6 and no skew slot	100	0.003	0.002	3.08	0.60	4.36	5.77
0.7 and no skew slot	100	0.004	0.003	0.81	0.08	2.76	3.85
0.8 and No skew slot	100	0.005	0.004	0.39	0.21	2.43	3.32
0.93 and no skew slot	100	0.006	0.004	0.76	3.15	4.39	5.90
0.93 and skew 0.25slot	100	0.007	0.006	0.56	1.96	2.57	3.38
0.93 and skew 0.5 slot	100	0.007	0.006	0.05	0.16	0.73	0.35
0.93 and skew 0.75 slot	100	0.01	0.009	0.26	1.01	1.22	1.45
0.93 and skew 1 slot	100	0.01	0.01	0.03	0.09	0.69	0.33

windward is weakened, while it is strengthened on the leeward side.

B. Analysis for the No-Load Voltage

In the harmonic analysis, the tooth harmonics should be considered. The ordinal number of tooth harmonics of voltage in the generator is

$$\nu = k2mq \pm 1 \tag{16}$$

where k is the order of tooth harmonic, m is the number of phases, and q is the number of the slots per pole per phase. In this paper, the ordinal number of first-order and second-order tooth harmonics are 8th, 10th, 17th, and 19th, respectively.

Because of the symmetry of the no-load line–line voltages $U_{\rm ab}, U_{\rm bc}$, and $U_{\rm ca}$, this paper only discuss $U_{\rm ab}$. The waveform and the spectrum of the no-load voltage are listed in Table III. Some results are presented in Figs. 6 and 7.

The earlier figures and tables indicate that, in scheme 1, $t_2/t_1 = 0.6$, the tooth harmonics of no-load waveform are large, and the waveform distortion occurs obviously. HDF and THF are 4.36% and 5.77%, respectively. The THF is 3.05 times of the upper limit in the GB/T 1029-2005, which is 1.5%. Without considering the slot skew, when the t_2/t_1 ratio increases from 0.6 to 0.93, the values of HDF and THF first decrease and then increase. When $t_2/t_1 = 0.8$, the values of HDF and THF are the minimum as 2.43% and 3.22%, respectively, and the waveform is the best of the four schemes without stator slot skew. When $t_2/t_1 = 0.93$, the values of HDF and THF are the maximum values as 4.39% and 5.90%, respectively, and the waveform is the worst of these schemes. These results indicate that by only changing t_2 without stator slot skew, the no-load voltage waveforms are not ideal. In scheme 3, which is the best design of the four schemes without stator slot skew, the value of THF is 2.15 times of the upper limit in the GB/T 1029-2005.

When $t_2/t_1 = 0.93$ and stator slot is skewed, the values of HDF and THF are reduced and the waveform is improved. In scheme 8, when the stator is skewed by one slot, the values of HDF and THF are the minimum values as 0.69% and 0.33%, respectively. In scheme 6, when the stator is skewed by 0.5 slot, the no-load waveform optimization is close to scheme 8. It means that, with simple manufacturing technique and low cost, the closest optimum no-load waveform is obtained in design scheme 6.

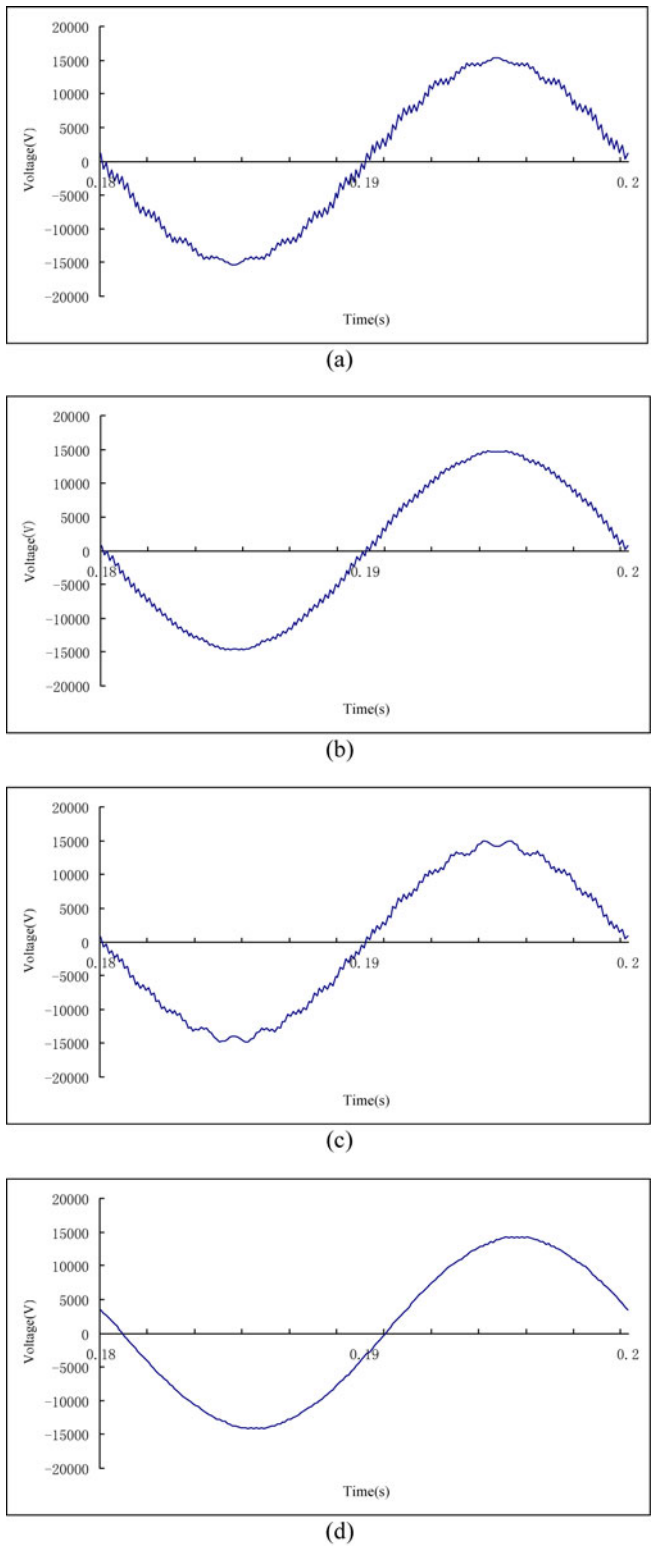

Fig. 6. Voltage waveforms at no load. (a) $t_2/t_1 = 0.6$ and no skew. (b) $t_2/t_1 = 0.8$ and no skew. (c) $t_2/t_1 = 0.93$ and no skew. (d) $t_2/t_1 = 0.93$ and 0.5 slot skewed.

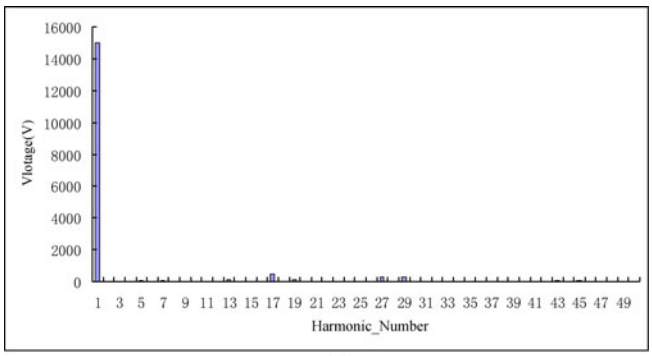

(a)

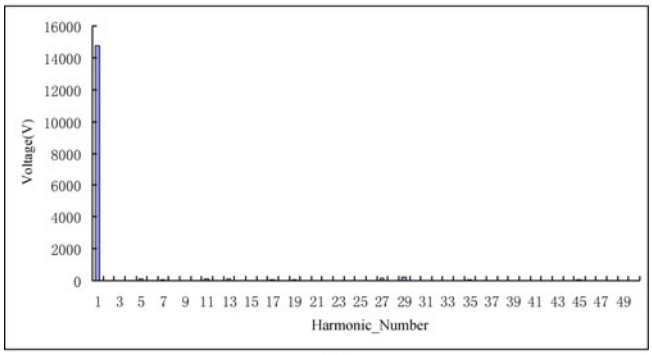

(b)

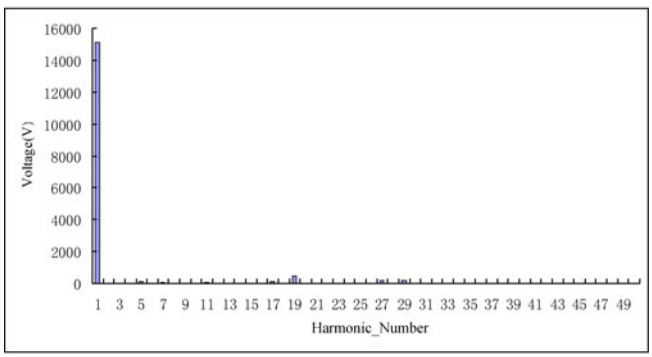

(c)

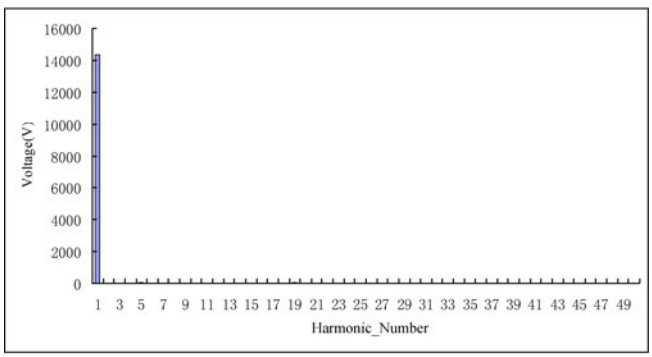

(d)

Fig. 7. Voltage harmonics at no load. (a) $t_2/t_1 = 0.6$ and no skew. (b) $t_2/t_1 = 0.8$ and no skew. (c) $t_2/t_1 = 0.93$ and no skew. (d) $t_2/t_1 = 0.93$ and 0.5 slot skewed.

Combining the harmonic results shown in Table III and spectrums in Fig. 7, it can be seen that only changing the value of t_2/t_1 without stator slot skew, the second-order tooth harmonic cannot be reduced effectively, especially in schemes 1 and 4; the percentage of the second-order tooth harmonic is the largest, which causes the worst waveform. When the design scheme of stator slot skew is adopted, the second-order tooth harmonic is reduced significantly, and then the optimized waveform is achieved, even if $t_2/t_1 = 0.93$.

Because the fractional slot stator windings can reduce the first-order tooth harmonic more effectively than the integral slot stator windings, the results show that the first-order tooth harmonics are very small for all the schemes. However, it cannot reduce the second-order tooth harmonic effectively, so the stator slot skewed schemes are adopted.

TABLE IV
LOSSES AND TEMPERATURES OF DAMPER BARS FOR DIFFERENT PITCHES

t_2/t_1	Loss (W)					Temperature (℃)	
	P_1	P_2	P_3	P_4	$\sum P$	$T_{\max}$	$T_{\min}$
0.6 and no skew slot	889	1498	621	172	3180	229.95	107.33
0.7 and no skew slot	1016	1169	494	130	2809	203.48	99.83
0.8 and No skew slot	1006	702	342	145	2195	183.26	90.80
0.93 and no skew slot	651	344	162	78	1235	147.99	78.17
0.93 and skew 0.25 slot	644	322	153	74	1193	146.96	77.64
0.93 and skew 0.5 slot	635	308	141	70	1154	145.86	77.13
0.93 and skew 0.75 slot	629	311	135	69	1144	145.34	76.98
0.93 and skew 1 slot	623	313	133	71	1140	144.85	76.86

C. Analysis for the Heat of Damper Bars

When the generator operates at the rated load, the results of losses and heat of damper bars are listed in Table IV. Some results are also presented in Fig. 8. For easy discussion, $P_1 - P_4$ and $\sum P$ are used to represent the losses of the first–fourth damper bars and the total losses of the damper bars, respectively. $T_{\max}$ and $T_{\min}$ are used to represent the maximum and minimal temperatures of damper bars, respectively.

Table IV and Fig. 8 show that the losses and heat of the first and second damper bars that are on the leeward are significantly larger than those of third and fourth damper bars that are on the windward. Because of the armature reaction, the distribution of the air gap magnetic field is distorted when the generator operates at the rated load. The magnetic field on the windward is weakened while it is strengthened on the leeward. Then, the eddy current and losses on the leeward are significantly larger than those on the windward. In addition, the dissipation condition on the leeward is weaker than that on the windward, and the dissipation condition on the middle profile is weaker than that on the end profile. Then, the maximum temperature is at the middle of damper bar which nears the leeward of the rotor pole.

Table IV and Fig. 8 also show that the losses and temperature decrease obviously with the increase of t_2, when t_1 keeps unchanged. Because of the uneven air gap of generator, when t_2

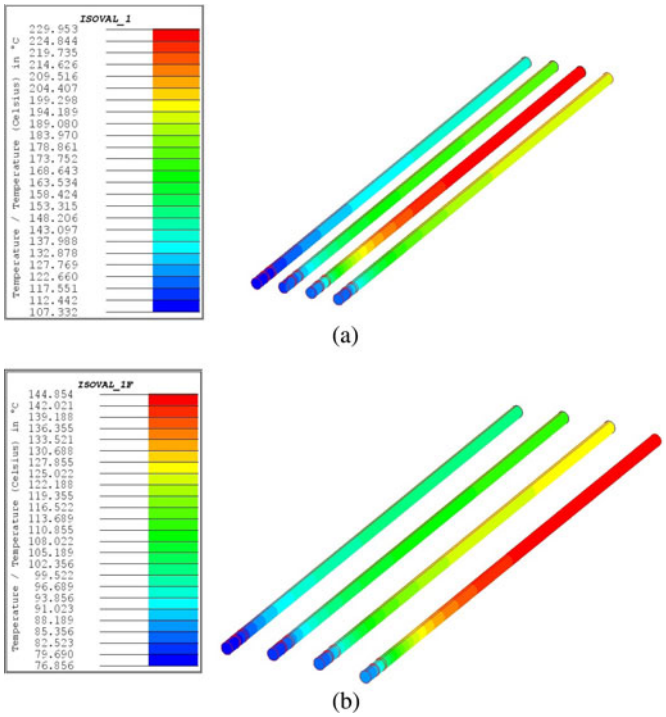

Fig. 8. Temperature distributions of damper bars with the rated load. (a) $t_2/t_1 = 0.6$ and no skew. (b) $t_2/t_1 = 0.93$ and 1 slot skewed.

increases, each damper bar becomes closer to the edge of pole and smaller eddy current is induced. Therefore, the losses and temperatures of the damper bars also decrease.

When $t_2/t_1 = 0.93$ and the stator slots are skewed, with the increase of skew degree, the damper bar loss further decreases. In scheme 8, the losses and heat of damper bars are reduced to the lowest. The reason of that is the stator skew slot can reduce the eddy current losses of damper bars, which are induced by the harmonic magnetic field. However, the effect of slot skew is limited on the reduction of damper bar loss and heat. It is not as obvious as the design scheme adjusts damper bar pitch. With the further comparison of different slot skew schemes, the difference of damper bar loss and heat is not great, especially for schemes 6 and 7, which are 0.5 slot skewed and 0.75 slot skewed, respectively, similar to scheme 8. It means that, with simple manufacturing technique and low cost, the closest lowest temperature of damper bar can be acquired.

It can be seen that the increase of the damper bar pitch and the stator slot skew can reduce the loss and heat of damper bars effectively. In this paper, by the comparison of scheme 8 and scheme 1, the total losses and maximum temperature are reduced by 64% and 37%, respectively. Considering the factors such as manufacture technique and cost, scheme 6 is the best.

From Table IV, it can be seen that at the rated load, the damper bar losses reduced by skewing the stator slot are small. Therefore, at the rated load, the effects of phase belt harmonics (fifth and seventh) on the loss of the damper bars are larger than that of tooth harmonics.

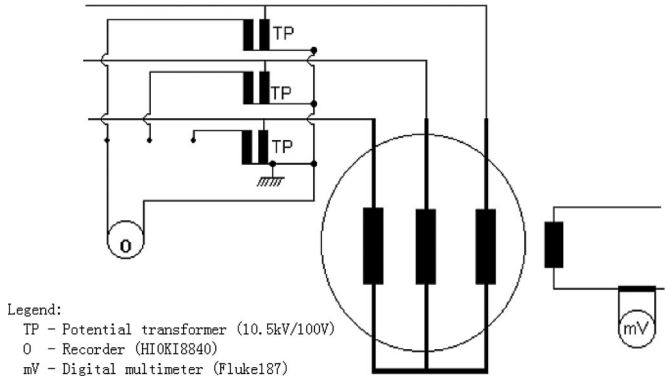

Fig. 9. Schematics of voltage waveforms test.

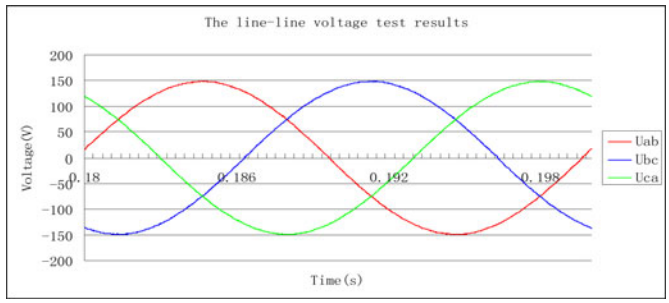

Fig. 10. Measured voltage waveforms at no load.

TABLE V
VERIFICATION OF RESULTS OF NO-LOAD VOLTAGE WAVEFORMS (U_{ab})

values	Harmonics of no-load voltage (%)					Voltage quality	
	1	8	10	17	19	*HDF*(%)	*THF* (%)
Calculated	100	0.007	0.006	0.05	0.16	0.73	0.35
Measured	100	0.006	0.004	0.07	0.15	0.71	0.34

TABLE VI
VERIFICATION OF RESULTS OF NO-LOAD VOLTAGE WAVEFORMS (U_{bc})

values	Harmonics of no-load voltage (%)					Voltage quality	
	1	8	10	17	19	*HDF*(%)	*THF* (%)
Calculated	100	0.043	0.034	0.086	0.460	0.81	0.52
Measured	100	0.038	0.036	0.089	0.355	0.77	0.34

TABLE VII
VERIFICATION OF RESULTS OF NO-LOAD VOLTAGE WAVEFORMS (U_{ca})

values	Harmonics of no-load voltage (%)					Voltage quality	
	1	8	10	17	19	*HDF*(%)	*THF* (%)
Calculated	100	0.056	0.044	0.079	0.469	0.85	0.61
Measured	100	0.052	0.038	0.083	0.432	0.71	0.34

D. Verification

To verify the correctness of the models, the no-load voltage measurement of generator is carried out for scheme 6. The test scheme is shown in Fig. 9.

The sampling time is set as 0.01 ms, and the harmonic frequency is taken at most 5 kHz. The results of no-load line–line voltage waveform are presented in Fig. 10 and Tables V–VII.

The comparison shows that the results of the simulation are close to the test results, and the differences between these three line–line voltages can be neglected.

TABLE VIII
TEST RESULTS OF AVERAGE TEMPERATURE OF FIELD WINDING

Average temperature of field winding (℃)	Calculated	Measured
	106	110
Environment temperature (℃)	47.6	

Since the damper bar is self-closed and, moreover, the generator is installed at the hydropower station for operation, the directly test of the temperature of damper bars is very difficult. However, the average temperature of field winding can be measured by the resistance method. So, according to the Chinese National Standard, the resistance method is adopted in this paper to test the average temperature of the field winding at the rated load condition. Although this method cannot prove the calculated damper bar temperature directly, it is the necessary first step to validating the damper bar temperatures indirectly. And the direct method to validating the damper bar temperatures is the task in the following study.

The measured average temperature of field winding is listed in the Table VIII, which includes the environment air temperature and the test result.

IV. CONCLUSION

For the tubular hydrogenerator in which the number of slots per pole per phase is less than 2, when the stator tooth pitch t_1 keeps unchanged, and only changing the pitch of damper bar t_2, the second-order tooth harmonic of no-load voltage cannot be reduced effectively.

When the stator pitch keeps unchanged, the change of the damper bar pitch influences the losses and heat of damper bars significantly. Increasing the ratio of t_2/t_1 can reduce the losses and heat of damper bar effectively.

Beside the methods mentioned earlier, the scheme of stator slot skew can achieve good no-load voltage waveform and reduce the losses and heat of damper bars.

Especially, compared with the design scheme which the stator core is skewed 1 stator slot, the another design scheme which the stator core is skewed 0.5 stator slot can simplify the manufacturing technique and reduce the cost, and can acquire the approximate optimum no load waveform and the lowest value of damper bar losses and heat.

The multislice moving electromagnetic field-circuit coupling model of the hydrogenerator and 3-D temperature field FE model of rotor are implemented, and the factors such as rotor motion and nonlinearity of the time-varying electromagnetic field, the anisotropic heat conduction of the rotor core lamination, and different heat dissipation conditions on the windward and leeward of the poles are considered. It can forecast the influences of different structure design schemes on the no-load voltage waveform of hydrogenerator and heat of damper bars. The research is helpful for enhancing the design quality and operation reliability of tubular hydrogenerators.

This tubular hydrogenerator has been operating safely all the times after it is installed at the hydropower station on July 2003. The good operating experience shows that the computing models and design results of this paper are reasonable.

ACKNOWLEDGMENT

The authors would like to thank Y. Guo, the Senior Member of the IEEE and an Associate Professor at the School of Electrical, Mechanical and Mechatronic Systems, Faculty of Engineering and Information Technology, University of Technology, Sydney, for his helpful revision of the paper.

REFERENCES

[1] C.-Y. Li, "The application of bulb-type hydro-generator set at low head hydropower station," *Developing*, no. 9, pp. 145–146, 2006.
[2] J.-B. Guo, "Analysis of damaged damping winding and magnetic pole in bulb type generator," *Chin. Power*, vol. 34, no. 7, pp. 63–67, May 2001.
[3] Z. Li, "Measurement of improving no-load voltage waveforms of salient-pole synchronous generator," *J. Harbin Inst. Electr. Technol.*, vol. 6, no. 3, pp. 1–16, Sep. 1983.
[4] C. E. Kim and J. K. Sykulski, "Harmonic analysis of output voltage in synchronous generator using finite element method taking account of the movement," *IEEE Trans. Magn.*, vol. 38, no. 2, pp. 1249–1252, Mar. 2002.
[5] H. Li, L. Li, and Y. Rang, "The effect of damper winding on the no-load voltage waveform of salient-pole synchronous generator," *Electr. Mach. Control*, vol. 7, no. 4, pp. 267–271, Nov. 2003.
[6] S. Keller, M. T. Xuan, and J.-J. Simond, "Computation of the no-load voltage waveform of laminated salient-pole synchronous generators," *IEEE Trans. Ind. Appl.*, vol. 42, no. 3, pp. 681–687, May/Jun. 2006.
[7] S. Wang, X. Wang, Y. Li, P. Su, W. Ma, and G. Zhang, "Steady-state performance of synchronous generators with ac and dc stator connections considering saturation," *IEEE Trans. Energy Convers.*, vol. 17, no. 2, pp. 176–182, Jun. 2002.
[8] A. M. Knight, H. Karmaker, and K. Weeber, "Prediction of damper winding currents and force harmonic components in large synchronous machines," in *Proc. 15th ICEM*, 2002, p. 35.
[9] A. M. Knight, H. Karmaker, and K. Weeber, "Use of a permeance model to predict force harmonic components and damper winding effects in salient pole synchronous machines," *IEEE Trans. Energy Convers.*, vol. 17, no. 4, pp. 478–484, Dec. 2002.
[10] G. Traxler-Samek, S. Lugand, and A. Schwery, "Add loss in the damper winding of large hydrogenerator at open-circuit and load conditions," *IEEE Trans. Ind. Electron.*, vol. 57, no. 1, pp. 154–160, Jan. 2010.
[11] S. Keller, M. Tu. Xuan, J.-J. Simond, and A. Chwery, "Large low-speed hydro-generator-unbalanced magnetic pulls and additional damper losses in eccentricity conditions," *IET Electr. Power Appl.*, vol. 21, no. 5, pp. 657–664, Sep. 2007.
[12] W. Li, Y. Zhang, and Y. Chen, "Calculation and analysis of heat transfer coefficients and temperature fields of air-cooled large hydro-generator rotor excitation windings," *IEEE Trans. Energy Convers.*, vol. 26, no. 3, pp. 946–952, Sep. 2011.
[13] H.-x. Xia, Y.-y. Yao, and G.-z. Ni, "Analysis of ventilation fluid field and rotor temperature field of a generator," *Electr. Mach. Control*, vol. 11, no. 5, pp. 472–476, Oct. 2007.
[14] M.-Q. Hu and X.-L. Huang, *Numerical Computation Method and its Application of Electric Machine Performance*. Nanjing, China: Southeast Univ. Press, 2003.
[15] F. Piriou and A. Razek, "Finite element analysis in electromagnetic systems accounting for electric circuits," *IEEE Trans Magn.*, vol. 29, no. 2, pp. 1669–1675, Mar. 1993.
[16] L.-x. Fu, *GB/T 1029-2005: The Test Measures of Three Phases Synchronous Machine*. Beijing, China: Standards Press of China, 2006.

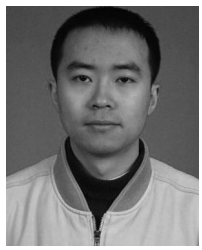

Zhen-nan Fan was born in Longchang, China, in 1981. He received the M.Sc. degree in electrical engineering from Chongqing University, Chongqing, China, in 2007. He is currently working toward the Ph.D. degree from the Department of Electrical Engineering, Chongqing University.

His current research interests include the magnetic and thermal field calculation of generators and the electrical machinery and motor drives.

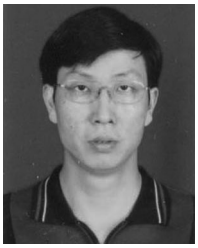

Yong Liao received the M.Sc. degree in electrical machinery and the Ph.D. degree in power system control from Chongqing University, Chongqing, China, in 1988 and 1997, respectively.

He is currently a Professor of electrical machinery and apparatus at Chongqing University. His current research interests include the magnetic and thermal field calculation of generators and the control of doubly fed electrical machines as used in renewable energy systems. In 1998, he participated in the Global Development Programme of Rockwell Automation, Milwaukee, WI. Between 2001 and 2002, he was a Visiting Professor at Norhtumbria University, UK.

Li Han received the M.Sc. and Ph.D. degrees in electrical machine from Chongqing University, Chongqing, China, in 1986 and 2008, respectively.

He is currently a Professor at Chongqing University. His current research interests include the field calculation and the design and control of electric machines.

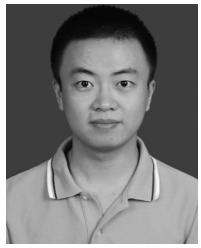

Li-dan Xie received the M.Sc. degree in electrical engineering from Chongqing University, Chongqing, China, in 2010.

He is currently an Engineer at Guodian Nanjing Automation Co. Ltd., Nanjing, China. His current research interests include the field calculation of generators and renewable energy.